Shared, unique and redundant functions of three members of the class I myosins (MyoA, MyoB and MyoF) in motility and chemotaxis in *Dictyostelium*

David L. Falk[1], Deborah Wessels[1], Leslie Jenkins[1], Tien Pham[1], Spencer Kuhl[1], Margaret A. Titus[2] and David R. Soll[1,*]

[1]W. M. Keck Dynamic Image Analysis Facility, Department of Biological Sciences, The University of Iowa, Iowa City, IA 52242, USA
[2]Department of Genetics, Cell Biology and Development, The University of Minnesota, Minneapolis, MN 55455, USA
*Author for correspondence (e-mail: david-soll@uiowa.edu)

Accepted 3 June 2003
Journal of Cell Science 116, 3985-3999 © 2003 The Company of Biologists Ltd
doi:10.1242/jcs.00696

Summary

Most cell types express two distinct forms of myosin I, amoeboid and short, distinguished by differences in their tail domains. Both types of myosin I have been implicated in the regulation of pseudopod formation in *Dictyostelium discoideum*. We examined three members of the myosin I family, one amoeboid, MyoB, and two short, MyoA and MyoB, for shared, unique and redundant functions in motility and chemotaxis. We used computer-assisted methods for reconstructing and motion analyzing cells, and experimental protocols for assessing the basic motile behavior of mutant cells in buffer and the responses of these cells to the individual spatial, temporal and concentration components of the natural wave of the chemoattractant cAMP. Analysis of both single and double mutants revealed that all three myosins play independent roles in suppressing lateral pseudopod formation in buffer and during chemotaxis. One, MyoB, also plays a unique role in priming cells to respond to the increasing temporal cAMP gradient in the front of a wave, while MyoF plays a unique role in maintaining the elongate, polarized shape of a cell in buffer, during chemotaxis in a spatial gradient of cAMP and in the front of a cAMP wave. Finally, MyoA and MyoF play redundant roles in the velocity response to the increasing temporal cAMP gradient in the front of a wave. These results, therefore, reveal an unexpected variety of shared, unique and redundant functions of the three class I myosins in motility and chemotaxis. Interestingly, the combined defects of the myosin I mutants are similar to those of a single mutant with constitutive PKA activity, suggesting that PKA plays a role in the regulation of all three class I myosins.

Key words: Basic cell motility, Chemotaxis, Myosin I, Myosin A, Myosin B, Myosin F, *Dictyostelium discoideum*, Functional redundancy

Introduction

Computer-assisted analyses of *Dictyostelium* amoebae translocating along a substratum in buffer have revealed that the basic motile behavior of a cell is surprisingly complex (Vawter-Hugart et al., 1994; Wessels et al., 1994; Wessels et al., 1996; Wessels et al., 1998; Chubb et al., 2002; Soll et al., 2003). Cells move cyclically, extending pseudopods on and off the substratum in a highly coordinated fashion in order to achieve persistent translocation interspersed with sharp turning (Wessels et al., 1994). Computer-assisted analyses have further revealed that the temporal and spatial dynamics of receptor occupancy lead to specific behavioral responses in the different phases of the natural chemotactic wave, adding to the complexity of cellular locomotion (Wessels et al., 2000a; Wessels et al., 2000b; Funamoto et al., 2001; Han et al., 2002; Soll et al., 2003; Zhang et al., 2003).

Actin plays a fundamental role in these complex behaviors, and an ever increasing number of actin-associated molecules and regulatory pathways have been implicated both in motor function, and in regulating the temporal and spatial dynamics of actin polymerization (Pollard et al., 2000; Small et al., 2002). One group of actin-based motor proteins implicated in the regulation of pseudopod formation during basic motile behavior is the family of myosin I proteins (Albanesi, 1985; Pollard and Korn, 1973; Zot et al., 1992; Uyeda and Titus, 1997; Mermall et al., 1998; Jung et al., 1993; Morita et al., 1996; Fukui et al., 1989). The class I myosins possess an N-terminal motor domain and a light chain binding neck region. The motor activity of the lower eukaryotic class I myosins is regulated by phosphorylation of a single serine or threonine in the TEDS rule site by a PAK family member kinase (Novak and Titus, 1997). There are two distinct types of myosin I, each distinguished by differences in their C-terminal tail domain. The tail of the 'amoeboid' form possesses a polybasic region that interacts with anionic phospholipids, then a domain typically rich in the amino acids glycine, proline alanine or glutamate (GPA) that binds actin, and an SH3 (*src* homology 3) domain. The 'short' forms of myosin I only possess a polybasic domain in their tail. *Dictyostelium* expresses seven class I myosins (Uyeda and Titus, 1997; de la Roche and Cote, 2001), three amoeboid (MyoB, MyoC and MyoD), two short (MyoA, MyoE and MyoF), and an additional tail-less form (MyoK).

The actin-based motor function of these myosins suggested

that they played roles in cellular locomotion. Because of their multiplicity, the possibility of functional redundancy has been entertained (Jung et al., 1993; Jung et al., 1996; Ostap and Pollard, 1996; Dai et al., 1999). If two forms of myosin I could substitute functionally for each other (i.e., if they were functionally redundant), then a null mutant of a single myosin I gene would exhibit no behavioral phenotype, while a double null mutant of the two myosin I genes would result in an aberrant phenotype, assuming similar levels of expression. Alternatively, if the two myosins could not substitute for each other (i.e., if they were not functionally redundant), then each individual null mutant would exhibit aberrant behavior, and the double null mutant would exhibit a combination of the aberrant behaviors, again assuming similar levels of expression.

The first computer-assisted analysis of cellular locomotion of a myosin I mutant (Wessels et al., 1991) was performed on a MyoB null mutant (Jung et al., 1990), lacking one of the three amoeboid myosins. It was demonstrated that when translocating in buffer, *myoB* mutant cells turned twice as frequently as control cells (Wessels et al., 1991). Since the extension of lateral pseudopods is responsible for the majority of sharp turns made by a cell crawling in buffer (Wessels et al., 1994), these results suggested that *myoB* mutant cells were defective in suppressing lateral pseudopod formation during basic motile behavior. MyoB has been shown to associate with the plasma membrane during locomotion (Senda et al., 2001), and has been localized to actin-rich regions, most notably the anterior pseudopod (Jung et al., 1996) and eupodia (Fukui and Inoue, 1997). It has also been shown to recruit components of the Arp 2/3 actin polymerization machinery to the plasma membrane through an interaction with an adapter protein, CARMIL (Jung et al., 2001), suggesting that it plays a role in regulating or focusing actin polymerization during pseudopod extension.

The second computer-assisted analysis (Titus et al., 1992) was performed on a null mutant lacking the short myosin I MyoA (Titus et al., 1989). Surprisingly, the behavioral defects of *myoA* mutant cells translocating in buffer were similar to those of *myoB* mutant cells (Titus et al., 1992), in spite of the differences between their overall structure. These results suggested that both MyoA and MyoB cooperated in a common process that suppresses lateral pseudopod formation and turning during cellular locomotion. In the case of *myoA* mutant cells, it was further demonstrated that the increase in lateral pseudopod formation was restricted to those pseudopods formed on the substratum, and that this defect was also manifested during chemotaxis (Titus et al., 1992).

We have extended our analysis of the roles of the class I myosins in the basic motile behavior of cells and chemotaxis. The two major questions to be addressed were (1) whether or not two distinct class I myosins (MyoA, MyoB) played functionally redundant roles during motility and (2) whether two similar class I myosins (MyoA, MyoF) played functionally redundant roles during motility. These questions have been addressed through a detailed analysis and comparison of single and double mutants. We have compared the three single mutants *myoA*, *myoB* and *myoF* and the two double mutants *myoA*/*myoB* and *myoA*/*myoF*, using computer-assisted methods to reconstruct and analyze the motion of cells (Soll, 1995; Soll and Voss, 1998; Heid et al., 2002) and experimental protocols to measure the behavior of individual cells in buffer, in response to natural waves of cAMP and in response to the spatial, temporal and concentration components of the natural wave (Wessels et al., 2000b; Soll et al., 2003; Zhang et al., 2002; Zhang et al., 2003). The results reveal an unexpected variety of shared, unique and redundant functions of the three class I myosins. Similarities between the defects exhibited by the five myosin I mutants analyzed here and a mutant expressing constitutive PKA activity suggest that PKA may play a role in the regulation of all three class I myosins.

Materials and Methods

Strains

The *myoA*, *myoB*, *myoF* and *myoA*/*myoB* mutants used in these studies were described previously (Titus et al., 1992; Titus et al., 1995; Novak et al., 1995). Strain nh6b is a non-homologous transformant selected as a control for comparison with the *myoA* mutant. The parental KAX3 cell line was used as a control for both the *myoB* and *myoA*/*myoB* mutant. The thymidine auxotroph JH10 strain was used as a control for the *myoF* mutant cells. The *myoA*/*myoF* mutant was generated by disrupting the *myoF* gene with the blasticidin resistance cassette in a *myoA* mutant previously generated in strain JH10 (Peterson et al., 1995) (S. Stephens and M.T., unpublished results). JH10 cells were used as controls for *myoA*/*myoF* mutant cells.

Strain maintenance and development

Spores of both control and mutant strains were stored in 10% glycerol at –80°C. For experimental purposes, cells were reconstituted every 3 weeks (Sussman, 1987). Cells were grown in 150 mm Petri dishes in HL-5 medium (Cocucci and Sussman, 1970) to confluency. To initiate development, cells were washed free of nutrients in basic salts solution (BSS: 20 mM KCl, 2.5 mM $MgCl_2$, 20 mM KH_2PO_4, pH 6.4), then dispersed at a density of 5×10^6 cells per cm^2 on filter pads (Soll, 1987). Filters were incubated in a humidity chamber and harvested for experimental purposes at the ripple state, which represents the onset of aggregation (Soll, 1979).

Analysis of basic motile behavior

The methods were similar to those previously described (Wessels et al., 2000b; Zhang et al., 2002; Zhang et al., 2003). Briefly, cells were washed from filter pads, diluted into BSS, and inoculated into a Sykes-Moore chamber (Bellco Glass, Vineland, NJ). The chamber was then perfused with BSS at a rate that replaced a chamber volume-equivalent of buffer every 15 seconds. Cell images were digitized into a Macintosh computer equipped with a frame-grabber at a rate of 4 frames per minute for 10 minutes for subsequent analysis.

Analysis of chemotaxis in a spatial gradient of cAMP

The methods were similar to those previously described (Varnum and Soll, 1984; Wessels et al., 2000b; Zhang et al., 2002; Zhang et al., 2003). Briefly, cells were dispersed on the bridge of a plexiglass chemotaxis chamber (Varnum and Soll, 1984; Zigmond, 1977). The bridge was bordered by two troughs, one containing BSS (sink) and the other containing 10^{-6} M cAMP in BSS (source). After 5 minutes, cell images were digitized into a Macintosh computer equipped with a frame-grabber at a rate of 4 frames per minute for 10 minutes for subsequent analysis. This period represents the time during which the spatial gradient of cAMP was steep enough to elicit a maximal response (Shutt et al., 1998).

Analysis of behavioral responses to the different phases of simulated temporal waves of cAMP

The methods were similar to those previously described (Varnum et al., 1985; Wessels et al., 1992; Wessels et al., 2000a; Zhang et al., 2002; Zhang et al., 2003). Briefly, cells were dispersed on the glass wall of a Sykes-Moore chamber. One port of the chamber was attached to a gradient maker and an opposing port to a peristaltic pump. To simulate the temporal dynamics of a wave, amoebae were perfused with 2 ml of BSS containing 8×10^{-9} M cAMP, then at 30-second intervals with 2 ml of BSS containing twice the concentration of cAMP to that of the previous solution. When the peak concentration of a natural wave (10^{-6} M) was reached, amoebae were perfused at 30-second intervals with 2 ml of BSS containing half the concentration of cAMP of the previous solution. This procedure was repeated four times, generating a sequence of four simulated temporal waves with a periodicity of 7 minutes. Cell behavior was recorded as described in previous sections for DIAS analysis.

Analysis of behavior in self-generated and wild-type-generated waves of cAMP

The methods for the analysis of cell behavior in response to self-generated waves were similar to those previously described (Escalante et al., 1997; Wessels et al., 2000b; Zhang et al., 2003). Briefly, 2 ml of a cell suspension at a density of 2.4×10^6 per ml were dispersed on the surface of a 35 mm plastic Petri dish. After 6 hours, cell images were continuously digitized at low magnification for a subsequent 6- to 9-hour period into a Macintosh computer at a rate of 6 frames per minute. Wave propagation was analyzed using the vector flow plot program of DIAS (Escalante et al., 1997; Soll, 1999; Zhang et al., 2003). The methods for the analysis of responses to wild-type-generated waves were similar to those previously described (Zhang et al., 2003). In brief, DiI-labeled mutant cells were mixed with unlabeled wild-type cells, plated on a 35 mm Petri dish and imaged through a NORAN laser scanning confocal microscope. Transmitted and fluorescent images were simultaneously collected every 20 seconds, averaged using Intervision software, and saved on the hard drive in Silicon Graphics format (SGI Inc., Mountain View, CA). SGI movies were then converted to QuickTime format, and the behavior of labeled and unlabeled cells analyzed.

Computer-assisted reconstruction and motion analysis of individual cells

The methods for digitizing video images, reconstructing cells as beta-spline representations, and motion analyzing the images with 2D-DIAS software have been described in detail in previous publications (Soll, 1995; Soll and Voss, 1998). For 2D analyses, cell perimeters were automatically outlined and converted to beta-spline replacement images. The centroid (center of area) of a cell at each time point was computed for each replacement image. Motility and dynamic shape parameters were computed from the cell centroid and contour, respectively (Soll, 1995; Soll and Voss, 1998).

Instantaneous velocity of a cell in frame *n* was computed by drawing a line from the centroid in frame *n*–1 to that in *n*+1 and dividing the length of the line by twice the interval time (15 seconds) between frames. For the analysis of instantaneous velocity as a function of developmental time, all cells in the population were motion analyzed. For all other experiments, motion analysis parameters were computed at 4-second intervals only for those cells crawling at instantaneous velocities above 2 μm per minute. For all strains in all tested situations, this represented over 70% of each population. Directional change was computed as the direction in the interval (*n*–1, *n*) minus the direction in the interval (*n*, *n*+1). Directional change values >180° were subtracted from 360°, providing a positive value between 0° and 180°. Maximum length was considered the longest chord between any two points along the perimeter of a cell. Maximum width was considered the longest chord at a 90° angle to the maximum length chord. Roundness was computed by the formula $100\times4\pi\times\text{area}/\text{perimeter}^2$. Chemotactic index (CI) in a spatial gradient of chemoattractant was the net distance moved directly towards the source of the chemoattractant divided by the total distance moved in the same time period. Percent positive chemotaxis was the proportion of the cell population exhibiting a positive CI over the period of analysis. A lateral pseudopod was considered to be a projection formed from the main axis of translocation at an angle ≥30° that attained a minimum of 5% total cell area and initially contained nonparticulate cytoplasm. The main axis of translocation was determined by drawing a line between the centroid of the cell in the frame 15 seconds earlier and the centroid of the cell in the present frame. Difference pictures were generated by superimposing the image in frame *n* on the image in frame *n*-1. The regions of the cell image in frame *n* not overlapping the cell image in frame *n*-1 were considered the 'expansion zones'. The period between overlapping images in difference pictures was 1 minute. 3D direct image reconstructions of living cells were performed by methods previously described (Wessels et al., 1998; Soll et al., 2000; Heid et al., 2002). In brief, thirty optical sections were collected in a 2 second period and repeated every 5 second. Images were obtained using differential interference contrast (DIC) microscopy. The edge of the cell in each optical section was automatically determined and only the image within the outline retained. These processed images were then stacked for each reconstruction and viewed.

Results

Strategy and protocols for analyzing mutant cell behavior

When *Dictyostelium* amoebae are starved, they acquire the machinery for cAMP-based chemotaxis. They employ this chemotactic system to attract up to 10^5 cells into an aggregate, the first step in a multicellular program leading to a sporangium (Loomis, 1982; Kessin, 2001). In the process of natural aggregation, precocious cells in a monolayer release pulses of the chemoattractant cAMP. Cells immediately centripedal to them respond by in turn releasing pulses of cAMP. This results in the relay of nondissipating, outwardly moving, symmetric waves of cAMP (Fig. 1A) (Tomchik and Devreotes, 1981), which pass across a cell at an average interval time of 7 minutes (Alcantara and Monk, 1974). In addition to relaying the wave outwardly, cells assess the spatial, temporal and concentration characteristics of the natural wave (Fig. 1A) in order to move towards the aggregation center (Soll et al., 2003). Aggregation-competent *Dictyostelium* amoebae are highly motile when perfused with buffer in the absence of chemoattractant and, therefore, do not require chemokinetic stimulation. When perfused with buffer, chemotactically responsive cells form lateral pseudopods and turn frequently, as if searching for direction (Soll et al., 2003). When challenged with relayed waves of cAMP, this basic cell behavior is manipulated in order to direct cells to aggregation centers. In the front of the wave, a cell experiences a positive spatial gradient of cAMP (concentration increasing in the direction of the aggregation center) and an increasing temporal gradient of cAMP (concentration increasing with time) (Fig. 1A). At the peak of the wave, a cell experiences a concentration of cAMP inhibitory to cellular translocation (Fig. 1A) (Varnum and Soll, 1984). In the back of the wave, a cell experiences a negative spatial gradient of cAMP (concentration decreasing in the direction of the aggregation center) and a decreasing temporal

A. Spatial, temporal and concentration characteristics of natural wave of cAMP.

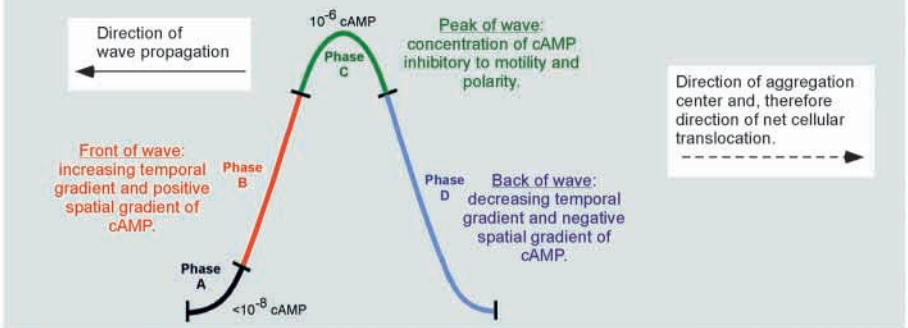

B. Protocols for testing the responses of cells to the different components of a wave.

Tested Characteristic	Behavior	Wave information	Test protocol
1. Basic motile behavior	Elongate morphology; rapid translocation; frequent lateral pseudopod formation; frequent turning.	Absence of chemotactic signal.	Perfusion with buffer in chamber.
2. Phase A of wave	Polarization in the direction of the aggregation center.	Positive spatial gradient of cAMP.	Spatial gradient of cAMP generated in spatial gradient chamber.
3. Phase B of wave	Surge in velocity; persistent, rapid translocation towards aggregation center; elongate morphology; suppression of lateral pseudopod formation and turning.	Increasing temporal gradient of cAMP.	Series of four simulated temporal waves of cAMP generated in a round perfusion chamber in the absence of spatial gradients.
4. Phase C of wave	Dramatic reduction in translocation; rounding up; retraction of dominant pseudopod.	High peak concentration of cAMP.	Same as #3.
5. Phase D of wave	Resumption of pseudopod formation but pseudopods are small and randomly directed; maintenance of apolarity and reduced translocation.	Decreasing temporal gradient of cAMP.	Same as #3.

Fig. 1. *Dictyostelium* amoebae respond in a unique fashion to four phases of the natural wave of cAMP (16, 17, 26, 31). (A) The spatial, temporal and concentration components of a relayed wave of cAMP in a natural aggregation territory. (B) The protocols for testing the behavior of mutant cells in buffer (i.e., 'basic motile behavior') and their responses to the different spatial, temporal and concentration components of a wave.

gradient of cAMP (concentration decreasing with time) (Fig. 1A). A cell responds in a unique fashion to each of four phases of a natural wave (Fig. 1B) (Soll et al., 2003). At the onset of the front of a natural wave (phase A), a cell polarizes in the direction of the aggregation center, presumably by assessing the direction of the spatial gradient of cAMP. In the middle two-thirds of the front of the natural wave (phase B), a cell suppresses lateral pseudopod formation and moves in a rapid, persistent, apparently blind fashion in the direction established in phase A, responding solely to the increasing temporal gradient of cAMP. At the peak of a natural wave (phase C), a cell stops translocating, begins to retract its anterior pseudopod and rounds up, in response to the high concentration of cAMP. In the back of a natural wave (phase D), a cell resumes pseudopod formation, but the pseudopods are reduced in volume and are extended in random directions. In the back of a natural wave, a cell remains apolar and, hence, does not translocate persistently in any one direction. The behavior in the back of the wave is in response to the decreasing temporal gradient of cAMP. This sequence of behaviors restricts translocation to phase B, preventing cells from chasing the spatial gradient in the back of the wave, which, in contrast to the front of the wave, increases in the direction away from the aggregation center.

To identify motility and chemotaxis defects in each myosin I mutant, a set of experimental protocols has been developed (Fig. 1B) (Wessels et al., 2000b; Zhang et al., 2002; Soll et al., 2003; Zhang et al., 2003). To assess basic motile behavior in the absence of a chemotactic signal, mutant cells were analyzed in a chamber in which they were perfused with buffer at a flow rate that excluded conditioning of the soluble microenvironment. To assess the capacity to read a positive spatial gradient, the presumed mechanism for determining polarity and the subsequent direction of translocation at the onset of the wave (phase A), cells were motion analyzed in a spatial gradient generated on the plexiglass bridge of a spatial gradient chamber (Fig. 1B) (Zigmond, 1977; Varnum and Soll, 1984). To assess the capacity of a cell to respond to the increasing temporal gradient of cAMP in the front of the wave (phase B), the high concentration of cAMP at the peak of the wave (phase C) and the decreasing temporal gradient of cAMP in the back of the wave (phase D), cells were treated with four temporal waves of cAMP that mimicked the approximate temporal dynamics and concentration range of a series of natural waves of cAMP (Fig. 1B) (Varnum et al., 1985; Wessels et al., 1992). These simulated temporal waves were generated in the absence of spatial gradients in a round perfusion chamber using gradient makers. To assess behavior during natural cell aggregation, homogeneous monolayers of cells were motion analyzed at low magnification (Escalante et al., 1997; Wessels et al., 2000b; Zhang et al., 2003). Finally, to assess responsiveness to the different phases of a natural wave generated by wild-type cells, mixed monolayers of vitally stained mutant cells and unstained wild-type cells at a ratio of 1:9, respectively, were imaged simultaneously through DIC microscopy and laser scanning confocal microscopy (Wessels et al., 2000b; Zhang et al., 2003). In each of the above protocols, the behavior of mutant cells was quantitatively compared to that of relevant control cells under identical conditions using DIAS software.

Basic motile behavior in buffer

2D-DIAS analysis of basic motile behavior in buffer revealed decreases in the mean instantaneous velocity of all three single myosin I mutants (*myoA*, *myoB*, *myoF*) and both double

Table 1. The basic motile behavior of myosin I null mutants assessed in buffer using 2D-DIAS

Cell type	Number of cells	Instantaneous velocity (μm/minutes)	Decrease in instantaneous velocity	Maximum length (μm)	Maximum width (μm)	Roundness (%)	Lateral pseudopod formation: One per 10 minutes (%)	Lateral pseudopod formation: More than two per 10 minutes (%)	Lateral pseudopod formation: Average number per 10 minutes	Lateral pseudopod formation: Increase in mutant per 10 minutes
Control (nh6b)	27	14.8±5.6		20±4	8±1	49±12	22	37	2.3	
myoA	15	9.8±4.0	34%	21±4	8±1	47±10	13	60	3.4	47%
P value*		0.0009		ns	ns	ns				
Control (KAX3)	30	12.7±3.5		20±3	9±1	46±7	10	50	2.5	
myoB	18	9.7±3.0	24%	23±4	10±2	40±11	0	94	4.1	64%
P value*		0.0016		0.0055	0.0308	0.0228				
Control (KAX3)	30	12.7±3.5		20±3	10±1	46±7	10	50	2.5	
myoA/myoB	24	7.8±2.9	38%	19±3	9±1	54±11	0	96	4.3	72%
P value*		0.0001		ns	0.0003	0.0017				
Control (JH10)	24	8.6±2.5		21±5	9±2	49±10	21	50	2.7	
myoF	71	7.2±2.4	16%	15±3	9±2	65±14	0	77	3.7	37%
P value*		0.0111		0.0001	ns	0.0001				
Control (JH10)	24	8.6±2.5		21±5	9±2	49±10	21	50	2.7	
myoA/myoF	24	5.0±1.3	42%	14±5	9±3	74±15	0	83	4.2	56%
P value*		0.0001		0.0001	ns	0.0001				

**P* value computed by Student's *t*-tests
Values are mean±s.e.m.

myosin I mutants (*myoA*/*myoB*, *myoA*/*myoF*) (Table 1). The percentage decrease in instantaneous velocity when compared to the relevant control strains ranged from 16% for the *myoF* mutant to 42% for the *myoA*/*myoF* mutant, and in all cases were statistically significant (Table 1). The extent of the observed decreases for the *myoA*, *myoB* and *myoA*/*myoB* mutants moving in buffer is similar to what was reported previously (Wessels et al., 1991; Titus et al., 1992; Novak et al., 1995). The decreases in instantaneous velocity were accompanied by increases in the frequency of lateral pseudopod formation for all five mutant strains (Table 1). The percentage increase ranged from 37% for the *myoF* mutant to 72% for the *myoA*/*myoB* mutant (Table 1). The decreases in instantaneous velocity were apparent in mutant cell perimeter tracks that were, on average, more contracted than those of relevant control cells (Fig. 2).

2D-DIAS analysis also revealed a major defect in cell shape in the *myoF* and *myoA*/*myoF* mutants not manifested in *myoA*, *myoB* or *myoA*/*myoB* mutant cells. The mean maximum length was reduced by 29% in *myoF* mutant cells and 33% in *myoA*/*myoF* mutant cells (Table 1). In addition, the mean roundness parameter was 36% higher in the *myoF* mutant cells and 51% higher in *myoA*/*myoF* mutant cells than in control cells (Table 1). A statistical analysis using the Student's *t*-test revealed that the defects in shape of *myoF* and *myoA*/*myoF* cells were significant (*P* values <0.05). A

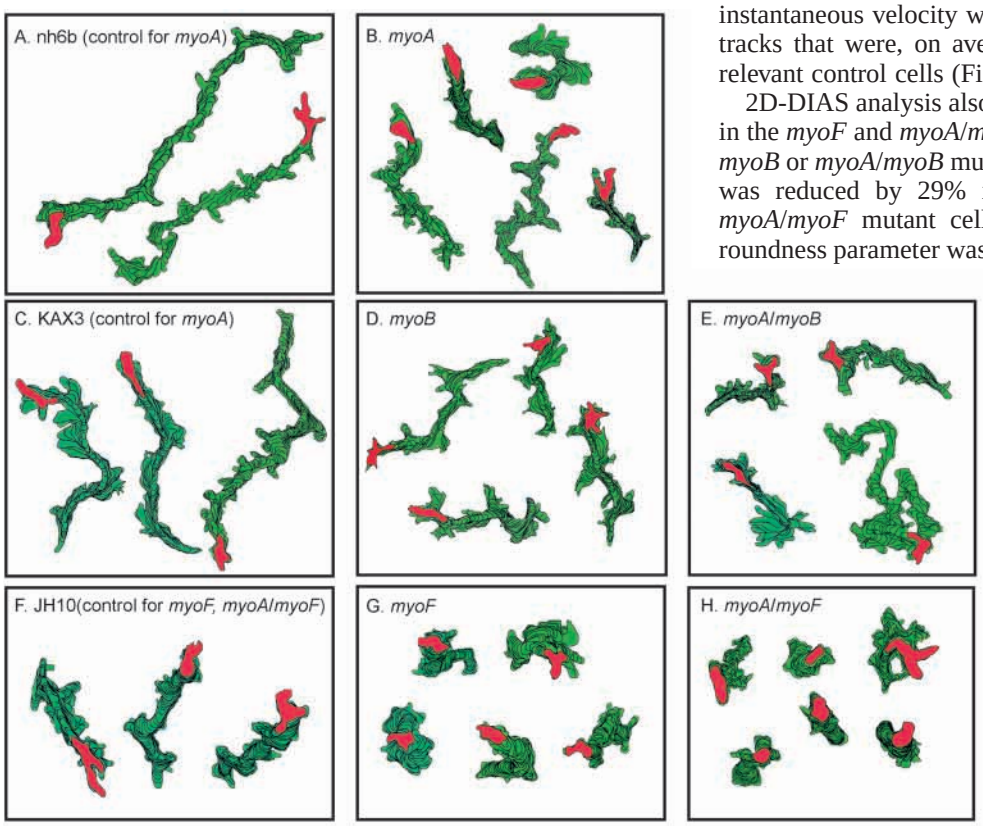

Fig. 2. All mutant cells translocate with reduced velocity, as revealed by perimeter tracks of representative control and mutant cells translocating on a glass surface while being perfused with buffer. The red-coded image represents the last cell image in each perimeter track. The interval time between images was 8 seconds, and the total time of analysis, 10 minutes for each cell.

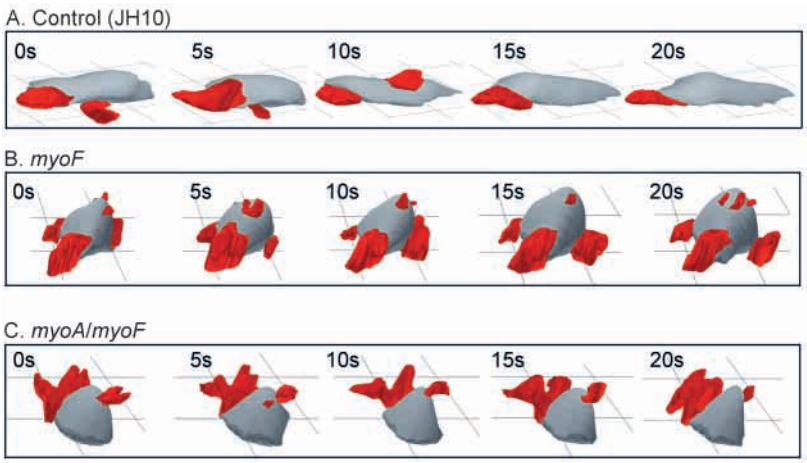

Fig. 3. The abnormal hemispherical shapes of *myoF* and *myoA*/*myoF* cells translocating in buffer revealed in 3D direct image reconstructions using 3D-DIAS software. (A) Representative control JH10 cell. **(**B) Representative *myoF* cell. **(**C) Representative *myoA*/*myoF* cell. Pseudopods were determined as regions lacking particulate cytoplasm and are color-coded red. Time is noted in seconds (s).

comparison of 3D-DIAS direct image reconstructions (Wessels et al., 1998; Soll, 1999; Soll et al., 2000; Heid et al., 2002) of control and mutant cells supported this conclusion. While representative JH10 cells translocating in buffer were long and flat, *myoF* and *myoA*/*myoF* mutant cells were rounder and hemispherical (Fig. 3). In contrast, 3D direct image reconstructions of *myoA*, *myoB* and *myoA*/*myoB* mutant cells were generally elongate and flat, like their relevant control cells (data not shown) and cells of control strain JH10 (Fig. 3A). In addition, *myoA*, *myoB* and *myoA*/*myoB* mutant cells also had mean length and width parameters similar to those of control cells and *myoA* and *myoB* cells had mean roundness parameters similar to control cells (Table 1). While the mean roundness parameter of *myoA*/*myoB* cells was significantly larger than that of control cells, the 3D morphology was similar to that of control cells and the roundness parameter was significantly lower than that of *myoF* and *myoA*/*myoF* cells.

These results demonstrate that MyoA, MyoB and MyoF each play a role in facilitating rapid cellular translocation and in suppressing lateral pseudopod formation in the absence of chemoattractant. There was no indication of functional redundancy, first because each single mutant exhibited a similar defect, and second because the cell defects of the double mutant were not significantly greater than those of the single mutant in the combination with the most severe defect (e.g., while the percentage decrease in instantaneous velocity was 38% for the *myoA*/*myoB* mutant, it was 34% for the single *myoA* mutant; and while the percentage decrease was 42% for the *myoA*/*myoF* mutant, it was 32% for the *myoA* mutant) (Table 1). In other words, the single mutant defects were not additive in the double mutants. The analysis of behavior in buffer also revealed that MyoF plays an additional, unique role in maintaining the elongate shape of cells translocating in buffer.

Chemotaxis in a spatial gradient of cAMP

Prior analysis of *myoA* mutant cells in a spatial gradient of cAMP revealed that they formed more lateral pseudopodia that contacted the substratum than control cells did (Wessels et al., 1996). While the *myoB* and *myoA*/*myoB* mutants were also found to translocate at lower velocities than control cells in buffer (Wessels et al., 1991; Novak et al., 1995), their behavior in a spatial gradient of cAMP was unknown. Thus, the motility of each mutant plus that of the *myoF* and *myoA*/*myoF* mutants in a spatial gradient of cAMP was analyzed. When wild-type cells are placed on the bridge of a spatial gradient chamber, the majority move in the direction of increasing cAMP concentration between 5 and 20 minutes of incubation, the time window during which the gradient is steep enough to elicit a positive chemotactic response (Shutt et al., 1998). There were strong average chemotactic indices (CI) for the three control cell lines, ranging from +0.47 to +0.76, and percent positive chemotaxis measurements ranging from 89 to 93% (Table 2). The mean CIs for all mutant cell lines were positive, ranging between +0.18 and +0.31 (Table 2), demonstrating that all were able to assess and move in a directed fashion up the cAMP gradient. However, the mean CI for every mutant was lower than that for each relevant control strain (Table 2). The reduction in CI varied from 52% for *myoA* cells to 76% for *myoA*/*myoB* cells (Table 2). A comparison of the histograms of chemotactic indicies revealed that cells of each of the five mutant lines were less efficient in attaining high-end chemotactic indices than relevant control cells (Fig. 4). In addition, all mutant cell lines had a lower proportion of cells with positive CIs than the relevant control cell lines (Table 2). Together these results demonstrate that cells of all five mutant lines were capable of responding positively up a spatial gradient of cAMP, but all were less efficient.

Since all mutant cell lines exhibited depressed instantaneous velocities and increases in the frequency of lateral pseudopod formation when translocating in buffer, the possibility was entertained that both of these defects were also manifested by mutant cells in a spatial gradient of cAMP, and were the cause in each case of the decrease in chemotactic efficiency. This proved to be the case. All mutant cell lines exhibited decreases in instantaneous velocity and increases in the frequency of lateral pseudopod formation in a spatial gradient of cAMP (Table 2). The increases in the frequency of lateral pseudopod formation varied from 54% for *myoF* to 240% for *myoA*/*myoB* mutant cells (Table 2). These defects in cell behavior were apparent in the perimeter tracks of mutant cells moving up spatial gradients of cAMP (Fig. 5). The perimeter tracks of mutant cells were more compressed and included more sharp turns than those of control cells.

These results demonstrate that although none of the class I myosins tested is essential for chemotaxis in a spatial gradient of cAMP, they all facilitate efficient chemotaxis. Since all of the single and double mutants exhibited similar behavioral defects either in a spatial gradient of cAMP or in buffer, it is likely that the decreases in chemotactic efficiency in both cases were due to the general incapacity to suppress lateral pseudopod formation. As in the analysis of behavior in buffer,

Table 2. The behavior of myosin I null mutants in spatial gradients of cAMP, assessed using 2D-DIAS

Cell type	Number of cells	Instantaneous velocity (μm/minutes)	Decrease in instantaneous velocity	Chemotactic index	Decrease in chemotactic index	Percent positive chemotaxis	Lateral pseudopod formation: One per 10 minutes (%)	Lateral pseudopod formation: More than 2 per 10 minutes (%)	Lateral pseudopod formation: Average number per 10 minutes	Lateral pseudopod formation: Increase in mutant
Control (nh6b)	35	9.2±3.1		+0.54±0.31		89	38	48	1.4	
myoA	28	7.2±2.7	22%	+0.26±0.32	52%	75	7	90	2.7	93%
P value*		0.0048		0.0045						
Control (KAX3)	27	13.4±6.5		+0.76±0.27		93	16	16	0.5	
myoB	28	6.9±2.9	49%	+0.31±0.33	59%	86	26	56	1.6	220%
P value*		0.0001		0.0001						
Control (KAX3)	27	13.4±6.5		+0.76±0.27		93	16	16	0.5	
myoA/myoB	24	6.1±2.9	55%	+0.18±0.49	76%	67	23	61	1.7	240%
P value*		0.0001		0.0001						
Control (JH10)	24	11.3±4.1		+0.47±0.33		92	35	44	1.3	
myoF	34	7.3±2.4	30%	+0.21±0.35	55%	63	27	62	2.0	54%
P value*		0.0001		0.0028						
Control (JH10)	24	11.3±4.1		+0.47±0.33		92	35	44	1.3	
myoA/myoF	22	6.0±2.8	47%	+0.20±0.37	57%	68	15	78	2.5	92%
P value*		0.0001		0.0065						

**P* values using Student's *t*-test.
Values are mean±s.e.m.

there was no indication of functional redundancy, since each single mutant exhibited a relatively similar defect, and these defects were not additive in double mutants (Table 2).

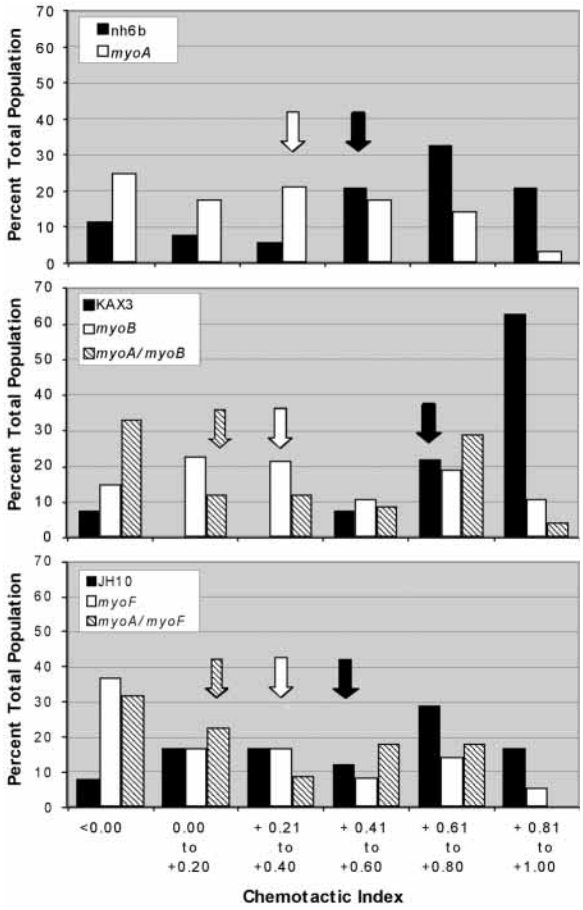

Fig. 4. Cells of all mutant strains are less efficient chemotactically than their relevant control cells. Histograms of (A) *myoA* cell and nh6b control cells; (B) *myoB*, *myoA*/*myoB* and KAX3 control cells; (C) *myoF*, *myoA*/*myoF* and JH10 control cells. Arrows refer to average chemotactic indices of respective strains.

Responses to the temporal and concentration components of the cAMP wave

When wild-type cells were challenged with four successive temporal waves of cAMP that roughly imitated the temporal dynamics of natural waves, but in the absence of spatial gradients, they rarely surged in the front of the first wave, but then exhibited velocity surges in the front of each of the last three waves (Varnum et al., 1985; Wessels et al., 1992; Wessels et al., 2000b; Zhang et al., 2002; Zhang et al., 2003). Velocity surges began at roughly the onset of the front of a wave and ended just prior to the peak of the wave. Cells of wild-type strains will exhibit clearly identifiable surges in the front of two or all of the last three in a series of four waves. All three control cell lines exhibited velocity surges on average in the front of the last three waves in a series of four temporal waves, as is evident in the time plot of velocity data averaged for a number of cells of each control strain (Fig. 6A-C; Table 3). The proportions of control cells that exhibited velocity surges in the front of each wave are presented in Table 3. The average proportions of control cells exhibiting surges in waves 2, 3 and 4 were 82%, 81% and 56%. For all three control cell lines (nh6, KAX3, JH10), cells in the front of the wave (phase B) were elongate, suppressed lateral pseudopod formation and translocated in a persistent fashion through the expansion of a dominant anterior pseudopod along the substratum, as is evident in pictures in which expansion zones are color-coded green (Fig. 6A-C – phase B). Cells at the peak of the wave (phase C) retracted their dominant pseudopod, rounded up and

Table 3. Velocity surges and turning in the front of temporal waves of cAMP

Cell type	Number of cells	Proportion of cells exhibiting a velocity surge in the front of			Average number of turns in front of wave*	Increase in turns per wave
		Wave 2	Wave 3	Wave 4		
nh6b	13	76%	82%	65%	0.79	–
KAX3	4	100%	75%	50%	1.17	–
JH10	17	69%	85%	54%	1.38	–
myoA	16	86%	93%	57%	2.15	172%
myoB	12	17%	50%	75%	1.57	34%
myoA/*myoB*	13	12%	63%	75%	2.74	134%
myoF	10	80%	90%	60%	2.15	56%
myoA/*myoF*	8	13%	0%	13%	2.43	76%

	P values†		
	Wave 2	Wave 3	Wave 4
myoA vs nh6b	ns	ns	ns
myoB vs KAX3	0.0029	ns	ns
myoA/*myoB vs* KAX3	0.0028	ns	ns
myoF vs JH10	ns	ns	ns
myoA/*myoF vs* JH10	0.0067	0.0000	0.054

Cells of each type were treated with four successive temporal waves of cAMP generated in the absence of a spatial gradient.

*Averaged for waves 2, 3 and 4. A turn was measured as a change in the direction of translocation that was greater than 30 degrees and included translocation in the new direction of at least a cell body length distance. Computed as increase (%) over relevant control.

†*P* values computed by chi-squared test.

stopped translocating (Fig. 6A-C – 204 to 220 seconds, phase C). Cells in the back of the wave (phase D) reinitiated pseudopod formation, but remained apolar, extending pseudopods of diminished volume in all directions (Fig. 6A-C – 232 to 352 seconds, phase C). Control cells made no net progress in any direction in the back of the wave.

The *myoA* mutant

Time plots of velocity data averaged for a number of *myoA* mutant cells revealed velocity surges in the front of the last three in a series of four temporal waves of cAMP (Fig. 7A), a response pattern similar to control cells (Fig. 6A; Table 3). However, *myoA* mutant cells formed more lateral pseudopods than control cells in the front of the wave (phase B), resulting, on average, in a less elongate shape than hb6b control cells (compare phase B in Fig. 7A with phase B in Fig. 6A). *myoA* mutant cells also turned approximately three times as frequently as control cells (nh6b) in the front of the wave (Table 3), presumably as a result of the increased frequency of lateral pseudopod formation. The shape changes of *myoA* mutant cells at the peak and in the back of waves were similar to those of control cells (compare phases C and D in Fig. 7A with phases C and D in Fig. 6A).

The *myoB* and *myoA*/*myoB* mutants

Time plots of velocity data

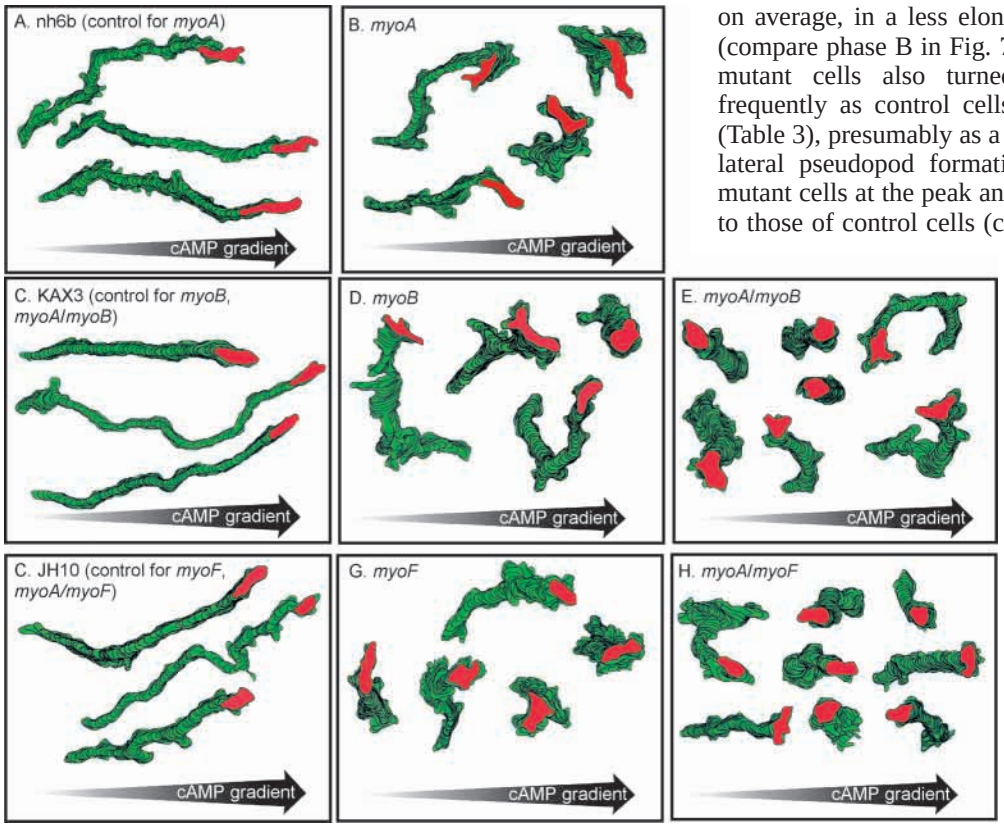

Fig. 5. Cells of all mutant strains react chemotactically in a spatial gradient of cAMP less efficiently and with reduced velocity, as revealed by perimeter tracks of representative control and mutant cells. The arrow at the bottom of each panel represents the direction of the increasing gradient of cAMP. The red-coded image represents the last in a perimeter track. The interval time between images is 8 seconds.

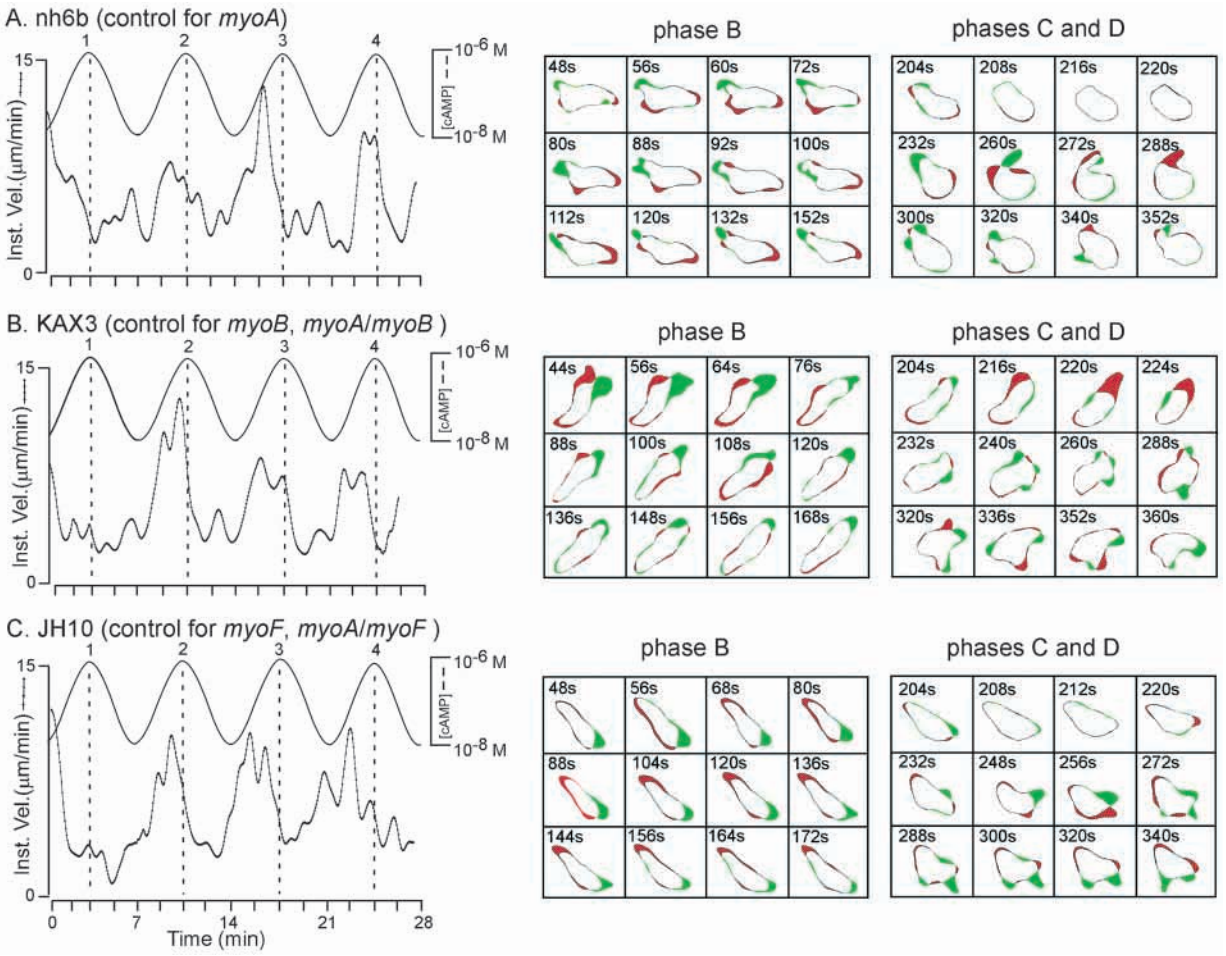

Fig. 6. All control strains responded normally to a series of four temporal waves of cAMP generated in the absence of spatial gradients of cAMP. In the first of each set of panels, the mean instantaneous velocity is plotted as a function of time for 10 cells treated with four successive waves of cAMP. The velocity surge occurs in each case in the front of the wave and ends as the wave reaches its peak (dashed lines). In the second two of each set of panels, difference pictures were generated during the front of the wave (phase B) and during the peak and back of the wave (phases C and D) for representative cells. The difference pictures for the peak of the wave (phase C) span the first four and those for the back of the wave (phase D) span the last eight of each set of difference pictures under the heading 'Phase C and D'. Green represents expansion zones and red contraction zones in the difference pictures.

revealed that both *myoB* and *myoA*/*myoB* mutant cells did not exhibit a velocity surge in either the first or second in a series of four temporal waves of cAMP (Fig. 7B,C). They did respond to the third and fourth wave (Fig. 7B). The delay in the response of *myoB* and *myoA*/*myoB* mutant cells is evident in the proportions of cells exhibiting velocity surges in each wave (Table 3). Like the *myoA* mutant cells, *myoB* and *myoA*/*myoB* mutant cells formed more lateral pseudopods than control cells when responding to the front of a wave (phase B in Fig. 7B,C), resulting on average in a less elongate shape than control cells (compare with phase B in Fig. 6B). *myoB* and *myoA*/*myoB* mutant cells also turned more frequently than control cells (KAX3) in the front of a wave (Table 3), presumably as a result of the increased frequency of lateral pseudopod formation. The shape changes of *myoB* and *myoA*/*myoB* mutant cells at the peak of the wave (204-216 seconds in Fig. 7B,C) and in the back of the wave (232-352 seconds in Fig. 7B,C) were similar to those of control cells (Fig. 6B). Hence, *myoA*/*myoB* mutant cells exhibited the defects of *myoB* cells.

The *myoF* mutant

Time plots of velocity data revealed that *myoF* mutant cells, like control and *myoA* mutant cells, responded normally to a sequence of four temporal waves of cAMP. The *myoF* mutant cells surged in the front of the last three in a series of four successive waves (Fig. 7D; Table 3). However, *myoF* mutant cells, like *myoA*, *myoB* and *myoA*/*myoB* cells, were less elongate than control cells when responding to the front of a wave and formed lateral pseudopods more frequently (phase B in Fig. 7D), resulting in a higher frequency of turns than control cells (Table 3). The *myoF* mutant cells responded normally to the peak and back of waves (phases C and D in Fig. 7D).

The *myoA*/*myoF* mutant

myoA/*myoF* mutant cells, in sharp contrast to *myoA* mutant, *myoF* mutant and control cells, did not surge in any of the four successive temporal waves of cAMP (Fig. 7E, Table 3). In the front of the last three in a series of four temporal waves, cells

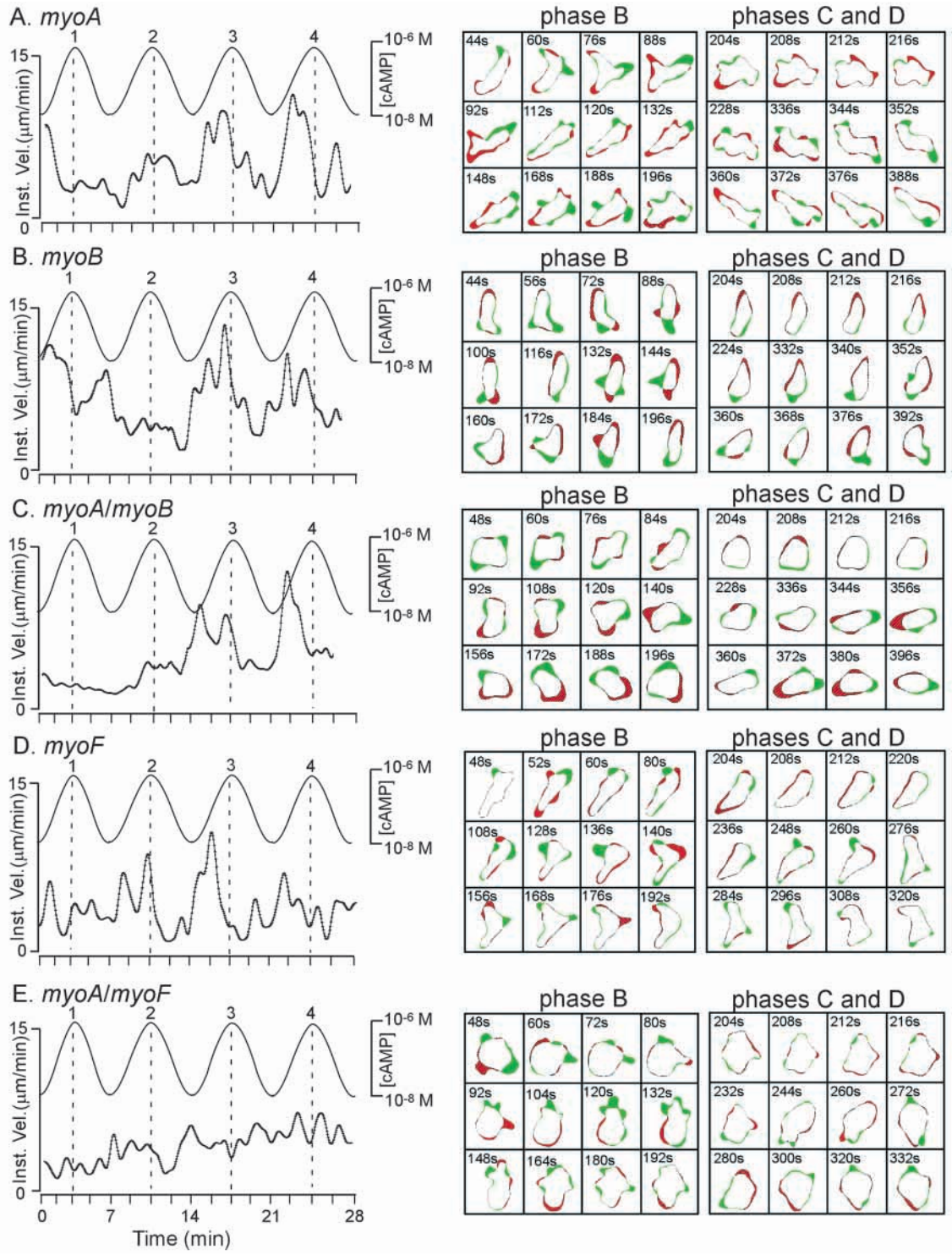

Fig. 7. Defects in responses to temporal waves were exhibited by *myoB*, *myoA*/*myoB* and *myoA*/*myoF* mutant cells. The velocity of mutant cells is plotted as a function of a series of four temporal waves of cAMP generated in the absence of spatial gradients of cAMP. For an explanation of panels and reconstructions, see legend to Fig. 6.

were less elongate and formed lateral pseudopods at frequencies higher than control cells (phase B in Fig. 6E), resulting in a higher frequency of turns (Table 3). The *myoA*/*myoF* mutant cells responded normally to the peak and back of waves (phase C and D in Fig. 7E).

Together, these results demonstrate, first, that the major behavioral defect manifested in buffer and in a spatial gradient of cAMP by all mutant cells, namely, an increase in the frequency of lateral pseudopod formation and turning, is also manifested in the front (phase B) of temporal waves of cAMP.

Table 4. Cyclic behavior, streaming and aggregation in natural aggregation territories

Strain	Aggregation in submerged cultures assessed at low magnification: Streams	Aggregation in submerged cultures assessed at low magnification: Size of aggregates	Cyclic behavior revealed by vector flow plots*: Onset of submerged pulsing in culture (hours)	Cyclic behavior revealed by vector flow plots*: Average periodicity ±s.d.
nh6b	Normal; large streams; good relay	Large	~6	10±1.9
myoA	Small streams break up; cells change direction frequently as they respond to competing aggregation centers	Small	~6	7.8±3.8
KAX3	Normal; large streams; good relay	Large	~6	8.1±1.6
myoB	Small streams break up; prevalence of competing centers	Small	~9	11.3±3.6
myoA/myoB	Small streams break up; prevalence of competing centers	Small	~7.8-8	7.6±2.9
JH10	Normal; large streams; good relay‡	Large‡	~7-7.5	5.4±1.0
myoF	Small streams break up; prevalence of competing aggregation centers	Small	~8-8.5	8.5±3.7
myoA/myoF†	Neg.	Neg.	Neg.	Neg.

*Assessed from the onset of pulsing until streaming.
†*myoA/myoF* cells do not exhibit cyclic behavior or aggregate. Therefore, all categories score negative (neg.).
‡JH10 cells from smaller stream and aggregates than control cells nh6b and KAX3, but they are larger than mutant *myoF* streams and aggregates.

Second, they suggest that MyoB, although not essential, facilitates priming of cells for the velocity response (surge) to phase B of a temporal wave. Third, they suggest that either MyoA or MyoF, both short myosins, is essential for the velocity response to phase B, and that the two can substitute for one another in this role. The fact that cells with either single deletion responded normally, but the double mutant did not respond at all, represents a clear case of functional redundancy.

Natural aggregation in homogeneous territories

The defects displayed by the single and double mutants in response to the various spatial and temporal components of the natural wave should impact natural aggregation. To test this prediction, cells were dispersed as a submerged monolayer on the surface of a plastic Petri dish (Escalante et al., 1997; Zhang et al., 2003). Cells of control strains nh6b and KAX3 began to aggregate after 6 hours, underwent streaming, rarely exhibited disruptions in the aggregation process within a territory and formed normal-sized, large aggregates (Table 4). Cells of the control strain JH10 began to aggregate after 7 hours, formed slightly smaller streams than the other two control strains, rarely exhibited disruptions in the aggregation process, and formed aggregates slightly smaller than those of the other two control strains (Table 4). The *myoA*, *myoB*, *myoA*/*myoB* and *myoF* mutant cell lines all exhibited the same characteristics in the natural aggregation process. Cells of the four mutant cell lines underwent aggregation, but all formed streams smaller than those of relevant control cells. The streams of all four mutants frequently fragmented (Table 4). Finally, all formed aggregates smaller than those of their relevant control strains (Table 4). In marked contrast to the other four mutant cell lines, *myoA*/*myoF* mutant cells neither streamed nor aggregated (Table 4).

In the process of natural aggregation, cells respond to outwardly moving nondissipating waves of cAMP by moving in surges towards the aggregation center. The surges are in response to the increasing temporal gradients in the fronts (phase B) of each successive wave relayed through the cell population (Thomchik and Devreotes, 1982; Soll et al., 2003). To test this characteristic in mutant cell lines, aggregating cell monolayers were videorecorded at low magnification after 6 hours of incubation. Selected regions of the monolayers were analyzed using vector flow technology (Escalante et al., 1997; Soll et al., 2000; Zhang et al., 2003). In vector flow plots the behavior of hundreds of cells in a small area are simultaneously vectored. Relative net movement of all cells in the selected area towards (+) or away from (–) the aggregation center are plotted. A cell responding correctly to a series of waves will exhibit a succession of peaks in the positive range with relatively constant periodicity. A cell moving randomly will exhibit a series of peaks randomly distributed in the positive and negative zone with erratic time intervals between peaks. All three control cell lines established surges (a series of positive peaks) towards the aggregation center with relatively constant periodicity after 6 to 7 hours of incubation (Table 4). An example of the vector flow plot of control cell line nhb6 is shown in Fig. 8A. The *myoA*, *myoB*, *myoA*/*myoB* and *myoF* mutant cell lines all established cyclic behavior (positive peaks in vector flow plot) with relatively constant periodicity after 6 to 9 hours of incubation (Table 4). In all of these mutant lines, there were frequent examples of transient disruption of cyclic behavior, sometimes followed by a change in vector direction. Examples of the vector flow plots of *myoA* and *myoF* mutant cells are shown in Fig. 8B and 8C, respectively. In marked contrast to the relevant control and other mutant cell lines, *myoA*/*myoF* mutant cells never established cyclic behavior (Table 4, Fig. 8D).

These results demonstrate that deletion of *myoA* alone, *myoB* alone, *myoF* alone or *myoA* plus *myoB* did not block the establishment of cyclic behavior, streaming or aggregation. However, in each mutant these aggregation-associated characteristics were less precise than in the relevant control cell lines, demonstrating that MyoA, MyoB and MyoF each plays a role in the precision of these processes. However, deletion of both *myoA* and *myoF* together resulted in a complete block in cyclic behavior, streaming and aggregation, a classic example of redundancy in which deletion of either gene alone does not

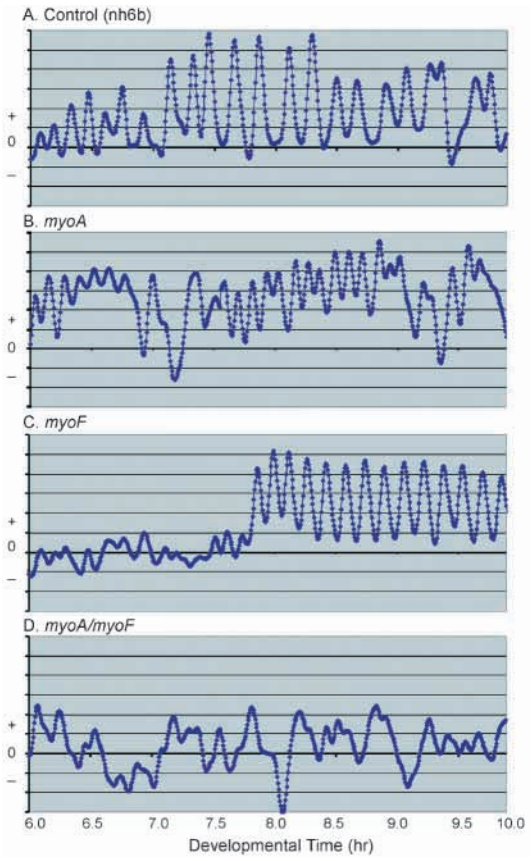

Fig. 8. Vector flow analysis of monolayers of control and mutant cells in natural aggregation territories. For each strain, a window of several hundred cells was monitored in a monolayer after 6 hours of incubation. In the vector flow plots, the magnitude of the vector components in the selected direction of the aggregation center were averaged and plotted over time for one control strain (nh6b), and mutant strains *myoA*, *myoF* and *myoA*/*myoF*. Because *myoA*/*myoF* cells did not aggregate, an arbitrary direction was selected. The *x*-axis represents time, and the *y*-axis the direction and extent of cell displacement. Displacement towards the aggregation center is positive and displacement away from the aggregation is negative. Note that while *myoA* and *myoF* cells initiate cyclic surges towards the aggregation center (positive displacement) in a manner similar to control cells, *myoA*/*myoF* cells do not initiate cyclic surges in any consistent direction.

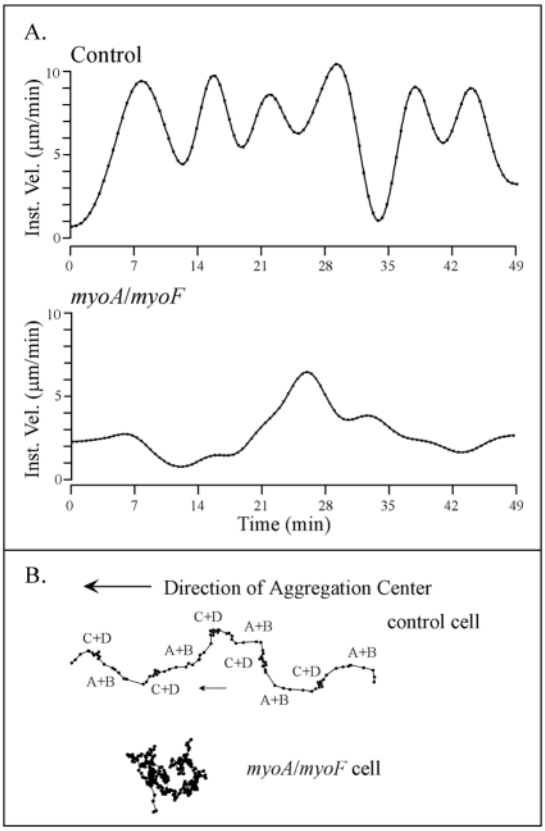

Fig. 9. *myoA*/*myoF* cells do not show any chemotaxis in natural waves of cAMP generated by control cells in mixtures. *myoA*/*myoF* cells were mixed with control (JH10) cells at a ratio of 1:9, respectively. After 8 hours, cells were motion analyzed. (A) Instantaneous velocity plots of a representative control and neighboring mutant cell. (B) Centroid tracks of a control cell and a neighboring *myoA*/*myoF* cell. The phases of the wave are noted along the tracks. The small arrow denotes direction of control cell.

block function, while simultaneous deletion of both genes completely blocks function. It should be noted that simultaneous deletion of both *myoA* and *myoB* resulted in the same minor defects observed in each of the single mutants, a classic example of the absence of redundancy.

Response of *myoA*/*myoF* mutant cells to natural wild-type waves

Cyclic behavior in a monolayer can only be established if a cell line is capable of emitting a pulsatile signal and responding to that signal in a cyclic fashion. All of the single myosin I mutants and the *myoA*/*myoB* double mutant could establish cyclic behavior in homogeneous submerged monolayers, demonstrating that each was capable of both pulsatile release of signal and cyclic surging in response to the signals. However, the *myoA*/*myoF* double mutant did not establish cyclic behavior. Hence, the *myoA*/*myoB* double mutant could be defective in either the pulsatile release of signal, the surging response to the signal, or both. To test whether *myoA*/*myoF* mutant cells were defective in the surging response, they were labeled with DiI, a fluorescent vital dye, and mixed with unlabeled control cells at a ratio of 1:9, respectively (Zhang et al., 2003). The cell mixture was then dispersed as a monolayer on a plastic tissue culture surface. Cell behavior was then monitored using simultaneous light microscopy to visualize all cells, and laser scanning confocal microscopy to distinguish mutant cells. The motions of labeled mutant cells and neighboring unlabeled control cells were then analyzed. Under these conditions, control cells generate outwardly moving, nondissipating waves of cAMP that pass across the minority of labeled mutant cells as well as the majority of neighboring control cells.

Control cells responded to the outwardly relayed waves with velocity surges readily identified in velocity plots (Fig. 9A). Neighboring *myoA*/*myoF* mutant cells did not respond to these waves with the same cyclic behavior (Fig. 9A). This defective behavior was evident in centroid tracks (Fig. 9B). While the

tracks of control cells included persistent stretches of centroids in the direction of the aggregation center (phases A and B) separated by more densely packed clusters of centroids (phases C and D), the entire track of a neighboring *myoA*/*myoF* cell was clustered and exhibited no net directionality (Fig. 9B). These results demonstrate that the redundant function of MyoA and MyoF is essential for the surging response to the front of successive waves of cAMP during natural aggregation, virtually the same defect observed in simulated temporal waves of cAMP (Fig. 7E).

Discussion

The multiplicity of class I myosins suggested that they may play a variety of unique roles in cell motility and chemotaxis. However, because of the structural similarities of members of this family, especially between short members and between amoeboid members, the possibility of functional redundancy had to be entertained. If two gene products are functionally redundant and equally expressed, then deletion of either (i.e., single mutants) would have little or no impact on the redundant function, while deletion of both (i.e. double mutant) would result in the loss of that function. Conversely, if two gene products are not functionally redundant, deletion of either would result in a loss of function. If the two gene products function in different processes, the deletion of both would result in defects in the two processes. If the two gene products function in the same general process, deletion of either should affect the same process and deletion of both should result in a defect no greater than the most extreme of the two single deletions. For the process of pinocytosis in *Dictyostelium*, functional redundancy has been demonstrated for MyoA and MyoB (an amoeboid and short myosin I), MyoB and MyoC (both amoeboid) and MyoB and MyoD (both amoeboid) (Novak et al., 1995; Jung et al., 1996). However, Novak et al. and Jung et al. presented data indicating that the roles of the three amoeboid myosins, MyoB, MyoC and MyoD, in facilitating rapid translocation were not redundant, and that MyoB and MyoC played nonredundant roles in phagocytosis. Dai et al. (Dai et al., 1999) presented data, which, when considered within the above interpretive framework, indicate that MyoA and MyoB play redundant roles in the genesis of cortical tension in suspended cells that have assumed a spherical shape. Using this interpretive framework, we have analyzed the *myoA*, *myoB* and *myoF* single null mutants, and the *myoA*/*myoB* and *myoA*/*myoF* double mutants to explore the functional relationships of these different myosins in pseudopod formation and chemotaxis. The results of this study reveal shared, unique and redundant roles for these three class I myosins in motility and chemotaxis.

Shared, nonredundant function

The original observations that the *myoA* and *myoB* mutants exhibited similar behavioral defects (Wessels et al., 1991; Titus et al., 1992; Wessels et al., 1996) in buffer were surprising. We have now added the *myoF* mutant to this list. Since individual null mutations of all three genes cause the same behavioral defects in buffer, namely a reduction in velocity and an increase in the frequency of lateral pseudopod formation, and the *myoA*/*myoB* and *myoA*/*myoF* double mutants exhibit similar defects that were nonadditive (i.e., were not the sum of the single mutant defects), we can tentatively conclude that all three myosins play nonredundant roles in the same behavioral process.

It seems reasonable to suggest that the increase in the frequency of lateral pseudopod formation exhibited by each of the five analyzed mutants in buffer resulted, at least in part, in the associated decreases in velocity, since an increase in the frequency of lateral pseudopod formation generally causes an increase in the frequency of turning, which in turn causes a decrease in centroid-based velocity measurements. This defect was manifested not only in buffer, but also during chemotaxis by all five mutant cell lines in spatial gradients of cAMP, the suggested mechanism for orientation in phase A of the natural wave (Fig. 1B) (Soll et al., 2003). In a spatial gradient of cAMP, each mutant was fully capable of assessing the direction of the gradient and moving in a directed fashion up it, but presumably because of the increased frequency of lateral pseudopod formation and turning, mutant cells did not stay on track, thus lowering the efficiency of chemotaxis. These defects (i.e., increased lateral pseudopod formation and decreased velocity) were also manifested by four of the mutant cell lines (*myoA*, *myoB*, *myoA*/*myoB*, *myoF*) that responded to increasing temporal gradients of cAMP with a velocity surge, the wave information that stimulates rapid movement towards the aggregation center in phase B of the natural wave (Fig. 1) (Soll et al., 2003). In an increasing temporal gradient of cAMP, each of these four mutant cell lines was able to establish surging, but each mutant continued to form pseudopods at increased frequency. This behavioral defect has been demonstrated in other mutants to reduce the net progress a cell makes towards an aggregation center in phase B of a natural wave, and hence the efficiency of natural aggregation, resulting in small aggregates in monolayers of developing cells (Wessels et al., 2000b; Zhang et al., 2003). This latter defect was also exhibited by the four myosin I mutants.

MyoF and MyoB play unique as well as shared roles

Our results demonstrate that in addition to the shared roles played by MyoA, MyoB and MyoF in the suppression of lateral pseudopod formation, MyoF and MyoB play unique roles in other cell functions related to polarity and motility. While *myoA*, *myoB* and *myoA*/*myoB* mutant cells were elongate like control cells, *myoF* and *myoA*/*myoF* mutant cells were constitutively hemispherical, suggesting that MyoF plays a role in the maintenance of the elongate cell shape. Our results also suggest that MyoB plays a unique role in the response to the front of a wave. In the normal behavioral response to a series of four temporal cAMP waves, a cell does not show a velocity surge in the front of the first wave, but does so in subsequent waves, suggesting that a normal cell must be ‘primed’ with the first wave in order to respond to subsequent waves. While *myoA* and *myoF* mutant cells exhibited a velocity surge in the last three of a series of four temporal waves, as do control cells, *myoB* and *myoA*/*myoB* mutant cells exhibited a velocity surge only in the last two in a series of four waves. In addition, the surge in the third wave was reduced, on average. These results suggest that MyoB plays a role in priming cells to respond to the front of a wave.

The SH3 domain of MyoB interacts with CARMIL, an

adaptor protein that binds to both subunits of capping protein and the Arp2/3 complex (Jung et al., 2001). CARMIL is localized to the leading edge of chemotaxing cells and mutants lacking this protein have reduced F-actin content and exhibit significant delays in streaming. The loss of MyoB might result in the inefficient recruitment of CARMIL to the leading edge which, in turn, could delay the response of the cell to the first two waves of cAMP. Another mechanism, perhaps requiring one of the two remaining amoeboid class I myosins, MyoC and MyoD, might then account for the response to the later waves of cAMP.

The *myoA*/*myoF* mutant reveals redundant function

While *myoA* and *myoF* mutant cells exhibited normal surges in response to the increasing temporal gradient in the front of the last three in a series of four temporal waves of cAMP, the *myoA*/*myoF* double mutant exhibited no surges. In addition, while *myoA* and *myoF* mutant cells established normal cyclic behavior in a homogeneous monolayer in response to self-generated cAMP waves, *myoA*/*myoF* mutant cells did not, and while *myoA* and *myoF* mutant cells aggregated, *myoA*/*myoF* mutant cells did not. These results suggest that MyoA and MyoF, both short class I myosins, perform the same function. Hence, when MyoA is deleted, MyoF fulfills that function and vice versa. However, when MyoA and MyoF are simultaneously deleted, there is complete loss of that function. Hence, they can substitute for one another in facilitating the surges in velocity in the front of a wave leading to cyclic behavior and aggregation in natural monolayers, and are, therefore, redundant. Our results also demonstrate that MyoB, an amoeboid myosin I, cannot substitute for either.

PKA and myosin I functions

pkaR mutant cells, which contain constitutively active PKA, translocate in buffer and in a spatial gradient of cAMP at approximately half the velocity of control cells, form lateral pseudopods at twice the frequency of control cells both in buffer and in a spatial gradient of cAMP, exhibit an average chemotactic index half that of control cells and do not suppress lateral pseudopod formation sufficiently in response to the increasing temporal gradient of cAMP in the front of a natural wave (Zhang et al., 2003). These defects are similar to the collective defects exhibited by the *myoA*, *myoB*, *myoA*/*myoB*, *myoF* and *myoA*/*myoF* myosin I mutants. *PkaR*$^{-}$ mutant cells also do not surge in the front of any in a series of four temporal waves of cAMP, a defect shared with the *myoA*/*myoF* double mutant. Finally, *pkaR* mutant cells are constitutively ovoid, a defect shared with *myoF* and *myoA*/*myoF* mutant cells. Normally, PKA activity is suppressed when wild-type cells are crawling in buffer or in the front of a natural wave, and activated at the peak of a natural wave, when the intracellular concentration of cAMP peaks (Behrens et al., 1996; Laub and Loomis, 1998).

The behavioral phenotype of the *pkaR* mutant has led to the proposal that PKA activity must be inhibited through its regulatory subunit in order for cells to attain the normal elongate morphology and suppress lateral pseudopod formation in a normal fashion in buffer, in a spatial gradient of cAMP and in response to the increasing temporal gradient in the front of a natural wave (Zhang et al., 2003). The similarity between the defects exhibited by the *pkaR* mutant and the combined defects of the five myosin I mutants suggest that the suppression of PKA activity is necessary for normal function of *myoA*, *myoB* and *myoF* mutants in buffer, in a spatial gradient of cAMP and in the front of a natural wave. Conversely, the activation of PKA at the peak of the wave would result in myosin I dysfunction. Consistent with this proposed regulatory scenario, we have found that all of the myosin I mutants, like the *pkaR* mutant, respond normally to the peak and back of the wave. This indicates that PKA may be a negative regulator of the class I myosins in *Dictyostelium*. This suggested link between PKA regulation and myosin I function in motility and chemotaxis warrants further exploration.

The authors are indebted to Dr K. Daniels for her help in generating figures and would like to thank Stephen Stephens for generating the *myoA*/*myoF* mutant. The research described here was supported by National Institutes of Health grants HD-18577 to D.R.S. and GM-46486 to M.A.T. The authors acknowledge the use of the W. M. Keck Dynamic Image Analysis Facility at The University of Iowa.

References

Albanesi, J. P., Fujisaki, H., Hammer, J. A., III, Korn, E. D., Jones, R. and Sheetz, M. P. (1985). Monomeric *Acanthamoeba* myosins I support movement in vitro. *J. Biol. Chem.* **260**, 8649-8652.

Alcantara, E. and Monk, M. (1974). Signal propagation in the cellular slim mould *Dictyostelium discoideum*. *J. Gen. Microbiol.* **85**, 321-324.

Behrens, M., Juliani, M. and Maia, J. (1986). Periodic changes in the cAMP-dependent protein kinase activity ratio in *Dictyostelium discoideum*. *Biochem. Int.* **13**, 221-226.

Chubb, J. R., Wilkins, A., Wessels, D. J., Soll, D. R. and Insoll, R. (2002). Pseudopodium dynamics and rapid cell movement in *Dictyostelium* Ras pathway mutants. *Cell Motil. Cytoskel.* **53**, 150-162.

Cocucci, S. and Sussman, M. (1970). RNA in cytoplasmic and nuclear fraction of cellular slime mold amoebas. *J. Cell Biol.* **45**, 399-407.

Dai, J., Ting-Beahl, H. P., Hochmuth, R. M., Sheetz, M. P. and Titus, M. A. (1999). Myosin I contributes to the generation of resting cortical tension. *Biophys. J.* **77**, 1168-1176.

de la Roche, M. A. and Cote, G. P. (2001). Regulation of *Dictyostelium* myosin I and II. *Biochim. Biophys. Acta.* **1525**, 245-261.

Escalante, R., Wessels, D., Soll, D. R. and Loomis, W. F. (1997). Chemotaxis to cAMP and slug migration in *Dictyostelium* both depend on MigA, a BTB protein. *Molec. Biol. Cell*. **8**, 1763-1775.

Fukui, Y. and Inoue, S. (1997). Amoeboid movement anchored by eupodia, new actin-rich knobby feet in *Dictyostelium*. *Cell Mot. Cytoskel.* **36**, 339-354.

Fukui, Y., Lynch, T. J., Brzeska, H. and Korn, E. D. (1989). Myosin I is located at the leading edges of locomoting *Dictyostelium* amoebae. *Nature* **341**, 328-331.

Funamoto, S., Milan, K., Meili, R. and Firtel, R. (2001). Role of phosphatidylinositol 3′ kinase and a downstream pleckstrin homology domain-containing protein in controlling chemotaxis in *Dictyostelium*. *J. Cell Biol.* **153**, 795-805.

Han, Y.-H., Chung, C., Titus, M., Wessels, D., Soll, D. and Firtel, R. (2002). Requirement of a vasodilator-stimulated phosphoprotein family member for cell adhesion, the formation of filopodia, and chemotaxis in *Dictyostelium*. *J. Biol. Chem.* **277**, 49877-49887.

Heid, P., Voss, E. and Soll, D. R. (2002). 3D-DIASemb: a computer-assisted system for reconstructing and behaviorally analyzing in 4D every cell and nucleus, and monitoring cytoplasmic flow in a developing embryo. *Develop. Biol.* **245**, 329-347.

Jung, G. and Hammer, J. A., III. (1990). Generation and characterization of *Dictyostelium* cells deficient in a myosin I heavy chain isoform. *J. Cell Biol.* **110**, 1955-1964.

Jung, G., Fukui, B, Martin, B. and Hammer, J. A. (1993). Sequence, expression pattern, intracellular localization, and targeting disruption of the *Dictyostelium* myosin I D heavy chain isoform. *J. Biol. Chem.* **268**, 14981-14990.

Jung, G., Wu, X. and Hammer, J. A., III (1996). *Dictyostelium* mutants lacking multiple classic myosin I isoforms reveal combinations of shared and distinct functions. *J. Cell Biol*. **133**, 305-323.

Jung, G., Remmert, K., Wu, X., Volosky, J. M. and Hammer, J. A. (2001). The *Dictyostelium* CARMIL protein links capping protein and the Arp2/3 complex to type I myosins through their SH3 domains. *J. Cell Biol.* **153**, 1479-1497.

Kessin, R. (2001). Dictyostelium – *Evolution, Cell Biology and the Development of Multicellularity.* Cambridge, UK: Cambridge Univ. Press.

Laub, M. and Loomis, W. (1998). A molecular network that produces spontaneous oscillations in excitable cells of *Dictyostelium*. *Molec. Biol. Cell* **9**, 3521-3532.

Loomis, W. F. (1982). The Development of *Dictyostelium*. San Diego, CA: Academic Press.

Mermall, V., Post, P. l. and Mooseker, M. (1998). Unconventional myosins in cell movement, membrane traffic, and signal transduction. *Science* **279**, 527-533.

Morita, Y. S., Jung, G., Hammer, J. A. and Fukui, Y. (1996). Localization of *Dictyostelium* myoB and myoD to filopodia and cell-cell contact sites using isoform-specific antibodies. *Eur. J. Cell Biol.* **71**, 371-379.

Novak, K. D. and Titus, M. A. (1997). Myosin I overexpression impairs cell migration. *J. Cell Biol.* **136**, 633-647.

Novak, K. D., Peterson, M., Reedy, M. and Titus, M. (1995). *Dictyostelium* myosin I double mutants exhibit conditional defects in pinocytosis. *J. Cell Biol*. **131**, 1205-1221.

Ostap, E. and Pollard, T. (1996). Overlapping functions of myosin-I isoforms? *J. Cell Biol*. **133**, 221-224.

Peterson, M., Novak, K., Reedy, M., Ruman, J. and Titus, M. (1995). Molecular genetic analysis of *myoC*, a *Dictyostelium* myosin I. *J. Cell Sci*. **108**, 1093-1103.

Pollard, T. D. and Korn, E. D. (1973). *Acanthamoeba* myosin I. Isolation from *Acanthamoeba castellani* of an enzyme similar to muscle myosin. *J. Biol. Chem.* **248**, 4682-4690.

Pollard, T., Blanchoin, L. and Mullins, R. (2000). Molecular mechanisms controlling actin filament dynamics in nonmuscle cells. *Annu. Rev. Biophys. Biomol. Struct*. **29**, 545-576.

Senda, S., Lee, S., Cote, G. and Titus, M. (2001). Recruitment of a specific amoeboid myosin I isoform to the plasma membrane in chemotactic *Dictyostelium* cells. *J. Biol. Chem*. **276**, 2898-2904.

Shutt, D. C., Jenkins, L. M., Carolan, E., Stapleton, J., Daniels, K., Kennedy, R. and Soll, D. R. (1998). T cell syncytia induced by HIV release T cell chemoattractants: demonstration with a newly developed single cell chemotaxis chamber. *J. Cell Sci*. **111**, 99-109.

Small, V., Stradal, T., Vignal, E. and Rottner, K. (2002). The lamellipodium: where motility begins. *Trends Cell Biol*. **12**, 112-120.

Soll, D. R. (1979). Timers in developing systems. *Science* **203**, 841-849.

Soll, D. R. (1987). Methods for manipulating and investigating developmental timing in *Dictyostelium discoideum*. In *Methods in Cell Biology* Vol. 28 (ed. J. Spudich), pp. 413-431. Orlando, FL: Academic Press, Inc.

Soll, D. R. (1995). The use of computers in understanding how animal cells crawl. *Int. Rev. Cytol.* **163**, 43-104.

Soll, D. R. (1999). Computer-assisted three-dimensional reconstruction and motion analysis of living, crawling cells. *Comp. Med. Imag. Graph*. **23**, 3-14.

Soll, D. R. and Voss, E. (1998). Two and three dimensional computer systems for analyzing how cells crawl. In *Motion Analysis of Living Cells* (ed. D. R. Soll and D. Wessels), pp. 25-52. John Wiley, Inc.

Soll, D. R., Voss, E., Johnson, O. and Wessels, D. J. (2000). Three-dimensional reconstruction and motion analysis of living crawling cells. *Scanning* **22**, 249-257.

Soll, D. R., Wessels, D., Zhang, H. and Heid, P. (2003). A contextual framework for interpreting the roles of proteins in motility and chemotaxis in *Dictyostelium discoideum.* Special *Dictyostelium* issue (ed. D. Manstein). *J. Musc. Res. Cell Motil.* **23**, 659-672.

Sussman, M. (1987). Cultivation and synchronous morphogenesis of *Dictyostelium* under controlled experimental conditions. In *Methods in Cell Biology*, vol. 28 (ed. J. A. Spundisch), pp. 9-24. New York: Academic Press.

Titus, M., Warrick, H. and Spudich, J. (1989). Multiple actin-based motor genes in *Dictyostelium*. *Cell Reg*. **1**, 55-63.

Titus, M., Wessels, D., Spudich, J. and Soll, D. R. (1992). The unconventional myosin encoded by the myo A gene plays a role in *Dictyostelium* motility. *Molec. Biol. Cell* **4**, 233-246.

Titus, M., Novak, K., Hanes, G. and Urioste, A. (1995). Molecular genetic analysis of *myoF*, a new *Dictyostelium* myosin I gene. *Biophys. J*. **68**, 152s-157s.

Tomchik, K. and Devreotes, P. (1981). Adenosine 3′,5′-monophosphate waves in *Dictyostelium discoideum*: a demonstration by isotope dilution-fluorography. *Science* **212**, 443-446.

Uyeda, T. and Titus, M. (1997). The myosins of *Dictyostelium*. In Dictyostelium: *A Model System for Cell and Developmental Biology* (ed. Y. Maeda, K. Inouye, I. Takeuchi), pp. 43-64. Tokyo, Japan: University Academy Press.

Varnum, B. and Soll, D. R. (1984). Effect of cAMP on single cell motility in *Dictyostelium*. *J. Cell Biol*. **99**, 1151-1155.

Varnum, B., Edwards, K. and Soll, D. R. (1985). *Dictyostelium* amoebae alter motility differently in response to increasing versus decreasing temporal gradients of cAMP. *J. Cell Biol*. **101**, 1-5.

Vawter-Hugart, H., Wessels, D., Voss, E., Minthorn, L., Murray, J. and Soll, D. R. (1994). Three dimensional motility cycles exhibited by leukocytes and *Dictyostelium discoideum*. *Cell Motil. Cytoskel. – Video Supplement* **4**, 362-364.

Wessels, D., Murray, J., Jung, G., Hammer, J. and Soll, D. R. (1991). Myosin IB null mutant of *Dictyostelium* exhibits abnormalities in motility. *Cell Motil. Cytoskel*. **20**, 301-315.

Wessels, D., Murray, J. and Soll, D. R. (1992). Behavior of *Dictyostelium* amoebae is regulated primarily by the temporal dynamics of the natural cAMP wave. *Cell Motil. Cytoskel*. **23**, 145-156.

Wessels, D., Vawter-Hugart, H., Murray, J. and Soll, D. R. (1994). Three dimensional dynamics of pseudopod formation and the regulation of turning during the motility cycle of *Dictyostelium*. *Cell Motil. Cytoskel*. **27**, 1-12.

Wessels, D., Titus, M. and Soll, D. R. (1996). A *Dictyostelium* myosin I plays a crucial role in regulating the frequency of pseudopods formed on the substratum. *Cell Motil. Cytoskel*. **33**, 64-79.

Wessels, D., Voss, E., von Bergen, N., Burns, R., Stites, J. and Soll, D. R. (1998). A computer-assisted system for reconstructing and interpreting the dynamic three-dimensional relationships of the outer surface, nucleus and pseudopods of crawling cells. *Cell Motil. Cytoskel*. **41**, 225-246.

Wessels, D., Reynolds, J., Johnson, O., Voss, E., Burns, R., Daniels, K., Garrard, E., O'Hallaran, T. and Soll, D. R. (2000a). Clathrin plays a novel role in the regulation of cell polarity, pseudopod formation, uropod stability and motility in *Dictyostelium. J. Cell Sci*. **113**, 26-36.

Wessels, D., Zhang, H., Reynolds, J., Daniels, K., Heid, P., Liu, S., Kuspa, A., Shaulsky, G., Loomis, W. F. and Soll, D. R. (2000b). The internal phosphodiesterase *RegA* is essential for the suppression of lateral pseudopods during *Dictyostelium* chemotaxis. *Molec. Biol. Cell* **11**, 2803-2820.

Zhang, H., Heid, P., Wessels, D., Daniels, K., Pham, T., Loomis, W. F. and Soll, D. R. (2003). The role of PKA in motility and chemotaxis. *Euk. Cell*. **2**, 62-75.

Zhang, H., Wessels, D., Fey, P., Daniels, K., Chisholm, R. and Soll, D. R. (2002). Phosphorylation of the myosin regulatory light chain plays a role in cell motility and polarity in *Dictyostelium* chemotaxis. *J. Cell Sci*. **115**, 1733-1747.

Zigmond, S. H. (1977). The ability of polymorphonuclear leukocytes to orient in gradients of chemotactic function. *J. Cell Biol.* **75**, 606-616.

Zot, H. G., Doberstein, S. K. and Pollard, T. D. (1992). Myosin-I moves actin filaments on a phospholipids substrate; implications for membrane targeting. *J. Cell Biol.* **116**, 367-376.